Graphene–Silver Hybrid Metamaterial for Tunable and High Absorption at Mid-Infrared Waveband

Shun Cao, Taisheng Wang, Qiang Sun, Yuguo Tang, Bingliang Hu, Uriel Levy, and Weixing Yu

***Abstract*— We proposed a hybrid metamaterial structure based on graphene-silver, which has tunable and efficient light-absorbing performance at the mid-infrared regime. It is shown that this model can absorb light effectively with a maximum of 100% at the absorption peak wavelength. In addition, the absorption peak wavelength can be adjusted flexibly by changing parameters, including the chemical potential applied to graphene or other structural parameters of the structure. This nearly perfect absorption capability is attributed to the synergetic effects of the localized surface plasmon enhancement of Ag nanoribbon, graphene plasmonics, metal–insulator–graphene mode and Fabry–Perot resonance. This kind of tunable absorber can be used in mid-infrared photodetectors or spectroscopy fields.**

***Index Terms*— Graphene, metamaterial, absorber, localized surface plasmon resonance enhancement, tunability.**

I. Introduction

OVER the past decades, metamaterials based perfect absorbers (MPAs) have been widely exploited for optoelectronic applications, including plasmonic biosensors [1]–[3], infrared thermal detection [4], [5], energy-harvesting devices [6]–[10]. Many MPAs with periodic nanostructures were proposed, which show a super absorptive property from visible to terahertz domain [11]–[14]. Noble metals, such as gold and silver, are widely used for the MPAs. Localized surface plasmon resonance (LSPR) excited by the metallic nanostructures is one of the main factors to enhance the interaction between the incident wave and the structure. However, the optical response of noble metals is passive and not easy flexible in tuning the absorption and resonating properties of the devices. This limits MPAs in applications such as spatial light modulators [15], [16].

In middle infrared and terahertz regime, graphene has prominent electric, optical properties and can behave like metals when it interacts with the incidence light and supports surface plasmons (SPs) [17]–[20]. This makes it useful in applications in transformation optics, tunable metamaterials, super-resolution and absorption enhancement [21]–[30]. Comparing with conventional metal SPs, graphene SPs can be tuned by electric gating or chemical doping and thus makes dynamically tunable resonant and active devices possible [31]–[33]. However, the absorption of graphene MPAs is relatively weak in the near-infrared range in that it is normally used as a lossy material without supporting SPs [34].

In view of the merits of noble metals and graphene, we proposed a graphene-based metamaterial absorber (GMA), which can support ultra-high absorption at the mid-infrared band. The finite-difference time domain (FDTD) method was employed to analyze GMA and the absorption of GMA is as high as 100% at wavelength of 4.55 μm. Additionally, the absorption mechanism of GMA is numerically studied and the effect of different parameters of GMA on the absorption was also discussed in detail.

II. Methods and Structure

Figure 1 show the proposed GMA structure which consists of Ag/SiO_2/graphene/Polyethylene oxide (PEO)/Ag nanoribbon and the geometric parameters of the GMA. Due to realize the extremely high value for the chemical potential in graphene, we chose the PEO, as dielectric material bewtten the top Ag nanoribbon and graphene. An ion gel, which consists an ionic liquid (e.g. Li^+) and a polymer (like PEO), can be realized in the experiments [35], [36]. The period of unit cells is 500 nm period in both x and y directions.

The model of graphene sheet was similar to and can be found in our previous work [25]. The graphene thickness was also assumed as 1 nm [37]–[40] in simulations, to make the numerical calculations reach proper convergence. In the simulation, the parameters of graphene are: Kelvin temperature $T = 300$ K, Fermi velocity $\nu_F = 10^5$ m/s, DC mobility $\mu = 10000\ \mathrm{cm^2V^{-1}s^{-1}}$, and the value of the chemical potential μ_c was tuned from 1.0 eV to 2.0 eV.

According to [25, eqs. (1)-(3)], the relative permittivity of graphene with different μ_c were calculated and shown

Manuscript received September 26, 2017; revised January 3, 2018; accepted January 29, 2018. Date of publication February 1, 2018; date of current version February 12, 2018. This work was supported in part by the Natural Science Foundation of China under Grant 61361166004 and Grant 61475156 and in part by the Science and Technology Department of Jilin Province under Grant 20140519002JH. *(Corresponding author: Shun Cao.)*

S. Cao and Y. Tang are with the CAS Key Laboratory of Bio-Medical Diagnostics, Suzhou Institute of Biomedical Engineering and Technology, Chinese Academy of Sciences, Suzhou 215163, China (e-mail: caoshunfy@163.com; tangyg@sibet.ac.cn).

T. Wang and Q. Sun are with the State Key Laboratory of Applied Optics, Changchun Institute of Optics, Fine Mechanics and Physics, Chinese Academy of Sciences, Changchun 130033, China (e-mail: wangtaisheng@sina.com; sunq@ciomp.ac.cn).

B. Hu and W. Yu are with the Key Laboratory of Spectral Imaging Technology, Xi'an Institute of Optics and Precision Mechanics, Chinese Academy of Sciences, Xi'an 710119, China (e-mail: hbl@opt.ac.cn; yuwx@opt.ac.cn).

U. Levy is with the Center for Nanoscience and Nanotechnology, Department of Applied Physics, Benin School of Engineering and Computer Science, The Hebrew University of Jerusalem, Jerusalem 91904, Israel (e-mail: ulevy@cc.huji.ac.il).

Color versions of one or more of the figures in this letter are available online at http://ieeexplore.ieee.org.

Digital Object Identifier 10.1109/LPT.2018.2800729

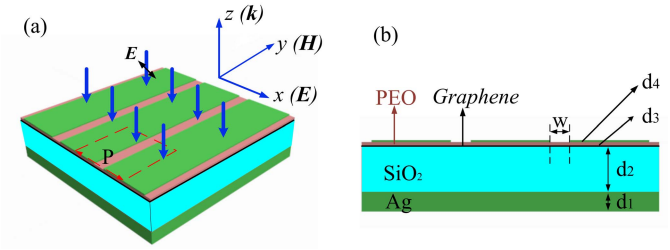

Fig. 1. The schematic diagram of the graphene-based metamaterial absorber with geometric parameters: P = 500 nm, w = 100 nm, d_1 = 100 nm, d_2 = 230 nm, d_3 = 20 nm, d_4 = 10 nm. (a) The perspective view and (b) the cross sectional view of the GMA.

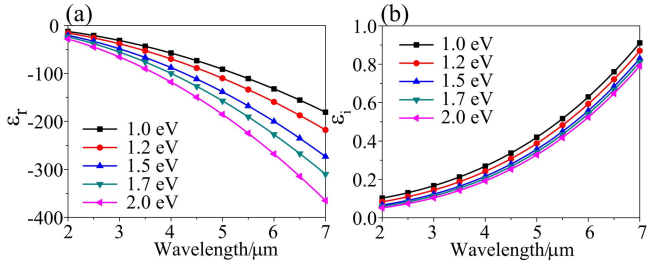

Fig. 2. Optical properties of graphene as a function of chemical potential in 2-7 μm waveband. (a) The real and (b) imaginary part of permittivity of graphene, respectively.

in Figs. 2(a) and 2(b), respectively. As shown in Fig. 2(a), a smaller μ_c results in a greater real part ε_r. However, the imaginary part changes slightly when the μ_c is increased, as depicted in Fig. 2(b).

By using the rigorous FDTD (Lumerical FDTD Solutions), the GMA structure was analyzed. The TM polarized plane wave at 4-6 μm waveband incident in z direction. The inset of Fig. 1(a) shows the direction of incident waves with respect of the perspective of the proposed absorber. Periodic boundary conditions (PBC) was employed in both x and y directions and perfectly matched layer (PML) boundary condition in z direction. The optical constants of Ag are taken from literature [41]. The refractive index of PEO can be obtained from [42]. We assumed the chemical potential μ_c of graphene is 1.7 eV and the relative permittivity was showed in Fig. 2.

The absorption was calculated by the equation $A(\lambda) = 1 - R(\lambda) - T(\lambda)$, $R(\lambda)$ is the reflection and $T(\lambda)$ is the transmission. Due to the thickness of the bottom Ag layer (100 nm) is much larger than its skin depth, there is nearly no transmittance in the waveband, i.e. $T(\lambda) = 0$. Under this condition, the absorptivity can be simplified into $A(\lambda) = 1 - R(\lambda)$.

III. Results and Discussion

Frequency-domain field and power monitors were used to investigate the S-parameters of GMA. Figure 3 shows the absorption spectra of GMA (the red curve) for the normal incident light. The absorption has one peak at wavelength of 4.55 μm, the corresponding absorption is 100%. In order to show the effect on absorption of graphene in GMA, we also calculated the structure without the graphene. The absorption of this structure (the green curve) was also shown in Fig. 3. In this case, the absorption has one peak at wavelength

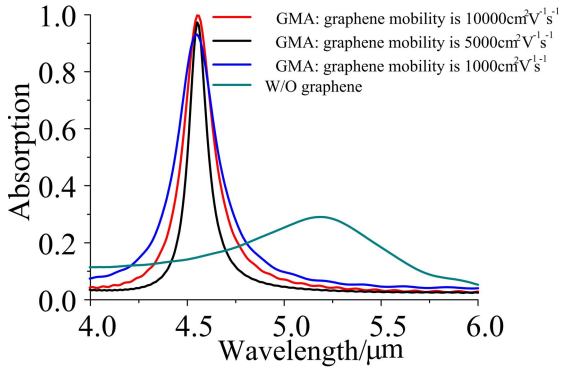

Fig. 3. Absorption spectra of GMA with graphene mobility 10000cm^{2}V^{-1}s^{-1} (red), GMA with graphene mobility 5000cm^{2}V^{-1}s^{-1} (black), GMA with graphene mobility 1000cm^{2}V^{-1}s^{-1} (blue) and GMA without graphene (green).

of 5.18 μm, however, the corresponding absorption is only 28.1%. As a result, it is confirmed that the graphene layer plays an important role in the enhancement of the absorption at this waveband. Electrolyte gates can be efficient at modulating the carrier concentration in graphene but also introduce high amount of scattering and the mobility in the layer is significantly reduced even down to 1000cm^{2}V^{-1}s^{-1} [43]. Due to the scattering effect of PEO, we also showed the absorption curves of graphene with a mobility of 1000cm^{2}V^{-1}s^{-1} and 5000cm^{2}V^{-1}s^{-1} (the black and blue line), respectively. From Fig. 3, the resonant wavelength of absorption peak is almost unchanged and the maximal absorption just decreased to 97.3% and 93.0% when the mobility of graphene is 5000cm^{2}V^{-1}s^{-1} and 1000cm^{2}V^{-1}s^{-1}, respectively. Therefore, the scattering, due to the PEO, does not have much effect on absorption.

The electric field distributions at different planes were calculated at wavelength of 4.55 μm (the absorption peak) and the results were shown in Figs. 4(a)-4(d). Figure 4(a) shows the distribution of the electric field at $y = 0$ μm plane. From the color bar, one can observe clearly that the electric field, located at the edges of upper Ag ribbon/PEO interface, is enhanced greatly with more than 50 factors. The detail of electric field distribution of Ag ribbon at $z = 124$ nm (3 nm above the Ag nano-ribbon) is shown in Fig. 4(b). One can find that the electric field is concentrated mainly at the edges of the Ag ribbon. This phenomenon can be attributed to the localized surface plasmon resonance (LSPR) effect [44]. Figure 4(c) shows the distribution of real E_z at $y = 0$ μm plane. As depicted in Fig. 2, at the waveband of 2-7 μm, the graphene shows a metal-like properties. Therefore, from Fig. 4(c), it can be found the SPs exist in the graphene layer. The PEO film, sandwiched by the Ag nano-ribbon and graphene, forms a sandwich nanocavity. The standing wave (SW) pattern of SPs exists in the nanocavity as shown in Figs. 4(a) and 4(c). Since the nanocavity functions as a cavity resonator for SPs, the electric field is enhanced greatly with more than 30 factors. This can be attributed to the hybrid Metal-Insulator-Graphene (MIG) plasmon mode, like MIM (Metal-Insulator-Metal) mode, due to the proximity of the graphene layer to the Ag grating. The incident wave could penetrate the graphene layer, which is a one-atom-thick material. The detail of electric

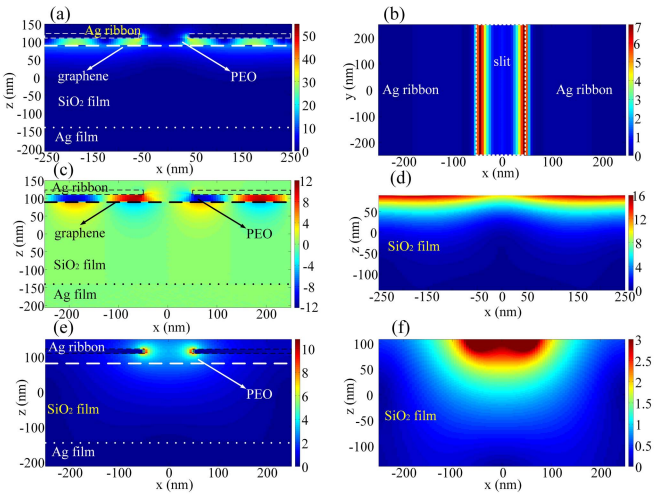

Fig. 4. (a) The distribution of the electric field of GMA in $y = 0$ plane. (b) The distribution of the electrical field at $z = 124$ nm plane. (c) The distribution of real z component of the electric field of GMA in $y = 0$ plane. (d) The detail of the distribution of the electric field in the SiO_2 film. (e) The distribution of the electric field of the simple Ag ribbon-PEO-SiO_2-Ag structure in $y = 0$ plane, with the same parameters of GMA. (f) The detail of the distribution of the electric field of the simple Ag ribbon-PEO-SiO_2-Ag structure in SiO_2 film.

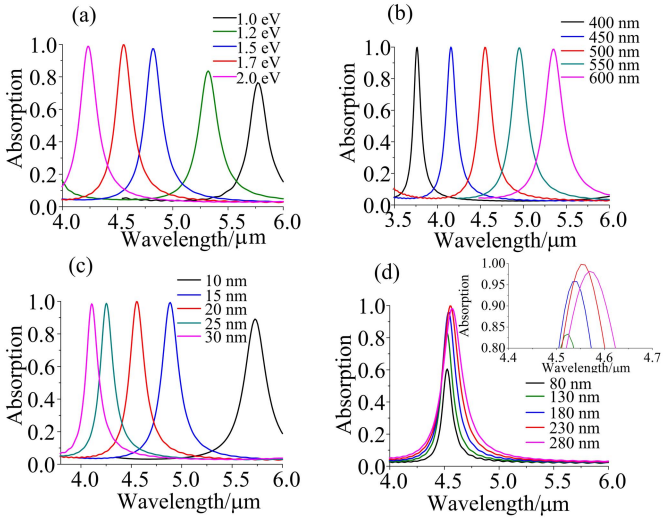

Fig. 5. The effect of different parameters of GMA on the absorption spectra: (a) chemical potential μ_c of graphene, (b) the period (P), (c) the thickness of the PEO (d_3) and (d) the thickness of the SiO_2 (d_2). The chemical potential of graphene is 1.7 eV in (b), (c) and (d).

field distribution of SiO_2 film at $y = 0$ μm in Fig. 4(a) is shown in Fig. 4(d). As shown in Fig. 4(d), the intensity of the electric field in the SiO_2 film is nearly zero close to the interface of the bottom Ag and SiO_2 film.

As a comparison, the electric field distribution of the GMA without graphene layer at y = 0 μm plane at wavelength of 5.18 μm was also calculated and shown in Figs. 4(e) and 4(f). From Fig. 4(e), the electric field is also concentrated mainly at the edges of the Ag nano-ribbon and the enhancement is only about 10 factors, which is much weaker than that of GMA with graphene. As shown in Fig. 4(f), due to lack of graphene plasmonics, there is no electric field enhancement in the SiO_2 film. As a result, the absorption of GMA without graphene is much lower than that of GMA with graphene.

Therefore, considering the results shown in Fig. 4 and the discussion mentioned above, one can conclude that the physical mechanism for the strong absorption of GMA is the synergistic effect of localized surface plasmon enhancement, graphene plasmonics and MIG mode. Firstly, localized surface plasmon enhancement was excited by the Ag nano-ribbon. And graphene SPs was generated by this electric field enhancement. Due to the very large imaginary part of the refractive index, the Ag and graphene absorbs the incident wave greatly [20]. Then Fabry–Pérot formed between the Ag grating and the Ag back reflector contributes to the absorption of remaining energy as well.

To further understand the absorption performance of GMA, the effect of different parameters including the chemical potential μ_c of graphene, the period (P) and the thickness of the PEO (d_3) and SiO_2 (d_2) on the absorption were studied and the results are shown in Fig. 5. Figure 5(a) shows the absorption versus wavelength for chemical potential μ_c of graphene. From Fig. 5(a), it can be observed that the change of μ_c has different effects on absorption and resonant wavelength. Specifically, the absorption peak wavelength has an obvious blue shift with the chemical potential μ_c increases. For absorption, when μ_c changes from 1.0 to 1.7 eV, the absorption increases from 76.4% to 100%. However, when μ_c further increases to 2.0 eV, the absorption reduces significantly to 97.5%. Therefore, one can tune the absorption performance of GMA by changing the chemical potential of graphene. Figure 5(b) shows the effect of the period (P) of GMA on the absorption. The period is changed from 400 to 600 μm with a step size of $\Delta P = 50$ μm. As can be seen, there is almost no change for the absorption when the period changes. The absorption peak wavelength has an obvious red shift with the period increases. The wavelength of absorption peak changes with a direct dependence on periodicity of GMA. This is consistent with the reference [45]. Figure 5(c) shows the absorption versus wavelength for different thickness of PEO (d_3), sandwiched by the Ag nano-ribbon and graphene. As shown in Fig. 5(c), it can be seen that the absorption peak wavelength has a blue shift with the thickness d_3 increases. For absorption, when d_3 changes from 10 to 20 nm, the absorption increases from 89.1% to 100%. However, when d_3 further increases, the absorption has almost no change, only reduces slightly to 98.8% (25 nm) and 98.4% (30 nm). From Figs. 5(a)-5(c), one can find that the absorption peak wavelength can be tuned flexibly by simply changing of the parameters including chemical potential of graphene, the period and the thickness of the PEO film. Therefore, the Ag nano-ribbon, PEO film and graphene are the resonant layer of GMA. The effect of the thickness of the SiO_2 film (d_2) on the absorption is shown in Fig. 5(d). It can be seen that there is almost no change for the absorption peak wavelength when the d_2 changes. To look into the details, the absorption curves at the peaks are magnified and shown in the inset of Fig. 5(d). One can find that the shifts of the resonant wavelength are no more than 0.05 μm. The absorption of GMA increases from 60.5% ($d_2 = 80$ nm) to 100% ($d_2 = 230$ nm). However, the absorption just reduces

slightly to 98.2% when d_2 further increases to 280 nm. The F–P vertical cavity are formed between the Ag grating and the bottom Ag film. Therefore, this effect originates from the vertical cavity between the top Ag nanoribbon and the Ag back reflector.

IV. Conclusion

In summary, we have proposed an efficient infrared graphene-based metamaterial absorber which can achieve an absorption of over 99%. The absorption property of GMA can be tuned easily by changing the chemical potential of graphene. The high absorptivity of the proposed hybrid absorber can be explained by the synergistic effect of the localized surface plasmon resonance enhancement, graphene plasmonics, MIG mode and F-P resonant. Our results can provide a valuable guide in applications including the design of plasmonic absorber and optical communications in the infrared range based on graphene.

References

[1] N. Liu, M. Mesch, T. Weiss, M. Hentschel, and H. Giessen, "Infrared perfect absorber and its application as plasmonic sensor," *Nano Lett.*, vol. 10, no. 7, pp. 2342–2348, 2010.

[2] K. Chen, R. Adato, and H. Altug, "Dual-band perfect absorber for multispectral plasmon-enhanced infrared spectroscopy," *ACS Nano*, vol. 6, no. 9, pp. 7998–8006, 2012.

[3] N. Li *et al.*, "DNA-assembled bimetallic plasmonic nanosensors," *Light, Sci. Appl.*, vol. 3, p. e226, Dec. 2014.

[4] T. Maier and H. Brückl, "Wavelength-tunable microbolometers with metamaterial absorbers," *Opt. Lett.*, vol. 34, no. 19, pp. 3012–3014, 2009.

[5] J. J. Talghader, A. S. Gawarikar, and R. P. Shea, "Spectral selectivity in infrared thermal detection," *Light, Sci. Appl.*, vol. 1, p. e24, Aug. 2012.

[6] S. Xiao, T. Wang, Y. Liu, C. Xu, X. Han, and X. Yan, "Tunable light trapping and absorption enhancement with graphene ring arrays," *Phys. Chem. Chem. Phys.*, vol. 18, pp. 26661–26669, Aug. 2016.

[7] C. F. Guo, T. Sun, F. Cao, Q. Liu, and Z. Ren, "Metallic nanostructures for light trapping in energy-harvesting devices," *Light, Sci. Appl.*, vol. 3, p. e161, Apr. 2014.

[8] S. A. Mann and E. C. Garnett, "Resonant nanophotonic spectrum splitting for ultrathin multijunction solar cells," *ACS Photon.*, vol. 2, no. 7, pp. 816–821, 2015.

[9] X.-C. Ma, Y. Dai, L. Yu, and B.-B. Huang, "Energy transfer in plasmonic photocatalytic composites," *Light, Sci. Appl.*, vol. 5, Feb. 2016, Art. no. e16017.

[10] C. Wu *et al.*, "Metamaterial-based integrated plasmonic absorber/emitter for solar thermo-photovoltaic systems," *J. Opt.*, vol. 14, no. 2, p. 024005, 2012.

[11] Q. Liang, T. Wang, Z. Lu, Q. Sun, Y. Fu, and W. Yu, "Metamaterial-based two dimensional plasmonic subwavelength structures offer the broadest waveband light harvesting," *Adv. Opt. Mater.*, vol. 1, no. 1, pp. 43–49, 2013.

[12] Z. H. Jiang, S. Yun, F. Toor, D. H. Werner, and T. S. Mayer, "Conformal dual-band near-perfectly absorbing mid-infrared metamaterial coating," *ACS Nano*, vol. 5, no. 6, pp. 4641–4647, 2011.

[13] H. R. Seren *et al.*, "Nonlinear terahertz devices utilizing semiconducting plasmonic metamaterials," *Light, Sci. Appl.*, vol. 5, p. e16078, May 2016.

[14] S. Cao *et al.*, "Meta-microwindmill structure with multiple absorption peaks for the detection of ketamine and amphetamine type stimulants in terahertz domain," *Opt. Mater. Exp.*, vol. 4, no. 9, pp. 1876–1884, 2014.

[15] C. M. Watts *et al.*, "Terahertz compressive imaging with metamaterial spatial light modulators," *Nature Photon.*, vol. 8, no. 8, pp. 605–609, 2014.

[16] X. Liu, T. Starr, A. F. Starr, and W. J. Padilla, "Infrared spatial and frequency selective metamaterial with near-unity absorbance," *Phys. Rev. Lett.*, vol. 104, no. 20, p. 207403, 2010.

[17] Z. Fang *et al.*, "Gated tunability and hybridization of localized plasmons in nanostructured graphene," *ACS Nano*, vol. 7, no. 3, pp. 2388–2395, 2013.

[18] Y. Cai *et al.*, "Enhanced spatial near-infrared modulation of graphene-loaded perfect absorbers using plasmonic nanoslits," *Opt. Exp.*, vol. 23, no. 25, pp. 32318–32328, 2015.

[19] F. Xiong, J. Zhang, Z. Zhu, X. Yuan, and S. Qin, "Ultrabroadband, more than one order absorption enhancement in graphene with plasmonic light trapping," *Sci. Rep.*, vol. 5, Nov. 2015, Art. no. 16998.

[20] S. Song, Q. Chen, L. Jin, and F. Sun, "Great light absorption enhancement in a graphene photodetector integrated with a metamaterial perfect absorber," *Nanoscale*, vol. 5, pp. 9615–9619, Aug. 2013.

[21] A. Vakil and N. Engheta, "Transformation optics using graphene," *Science*, vol. 332, no. 6035, pp. 1291–1294, 2011.

[22] V. Apalkov and M. I. Stockman, "Proposed graphene nanospaser," *Light, Sci. Appl.*, vol. 3, p. e191, Jul. 2014.

[23] L. Ju *et al.*, "Graphene plasmonics for tunable terahertz metamaterials," *Nature Nanotechnol.*, vol. 6, no. 10, pp. 630–634, 2011.

[24] N. Papasimakis, S. Thongrattanasiri, N. I. Zheludev, and F. J. G. Abajo, "The magnetic response of graphene split-ring metamaterials," *Light, Sci. Appl.*, vol. 2, p. e78, Jul. 2013.

[25] S. Cao, T. Wang, Q. Sun, B. Hu, U. Levy, and W. Yu, "Graphene on meta-surface for super-resolution optical imaging with a sub-10 nm resolution," *Opt. Exp.*, vol. 25, no. 13, pp. 14494–14503, 2017.

[26] L. Zhu *et al.*, "Angle-selective perfect absorption with two-dimensional materials," *Light, Sci. Appl.*, vol. 5, p. e16052, Mar. 2016.

[27] M. M. Jadidi *et al.*, "Tunable terahertz hybrid metal-graphene plasmons," *Nano Lett.*, vol. 15, no. 10, pp. 7099–7104, 2015.

[28] Y. Zhang, Y. Feng, B. Zhu, J. Zhao, and T. Jiang, "Graphene based tunable metamaterial absorber and polarization modulation in terahertz frequency," *Opt. Exp.*, vol. 22, no. 19, pp. 22743–22752, 2014.

[29] Y. Zhang *et al.*, "Independently tunable dual-band perfect absorber based on graphene at mid-infrared frequencies," *Sci. Rep.*, vol. 5, Dec. 2015, Art. no. 18463.

[30] S. Lee, T. Q. Tran, M. Kim, H. Heo, J. Heo, and S. Kim, "Angle- and position-insensitive electrically tunable absorption in graphene by epsilon-near-zero effect," *Opt. Exp.*, vol. 23, no. 26, pp. 33350–33358, 2015.

[31] M. Liu *et al.*, "A graphene-based broadband optical modulator," *Nature*, vol. 474, no. 7349, pp. 64–67, May 2011.

[32] Y. Bao, S. Zu, Y. Zhang, and Z. Fang, "Active control of graphene-based unidirectional surface plasmon launcher," *ACS Photon.*, vol. 2, no. 8, pp. 1135–1140, 2015.

[33] C. Liu, X. He, Z. Zhao, F. Lin, F. Liu, and W. Shi, "Tunable graphene near-IR dielectric loaded waveguides," *J. Phys. D, Appl. Phys.*, vol. 49, no. 26, p. 265102, 2016.

[34] J. Zhu, Q. H. Liu, and T. Lin, "Manipulating light absorption of graphene using plasmonic nanoparticles," *Nanoscale*, vol. 5, pp. 7785–7789, Jul. 2013.

[35] D. K. Efetov and P. Kim, "Controlling electron-phonon interactions in graphene at ultrahigh carrier densities," *Phys. Rev. Lett.*, vol. 105, no. 25, p. 256805, 2010.

[36] J. H. Cho *et al.*, "Printable ion-gel gate dielectrics for low-voltage polymer thin-film transistors on plastic," *Nature Mater.*, vol. 7, no. 11, pp. 900–906, Nov. 2008, doi: 10.1038/nmat2291.

[37] H. Hu *et al.*, "Far-field nanoscale infrared spectroscopy of vibrational fingerprints of molecules with graphene plasmons," *Nature Commun.*, vol. 7, Jul. 2016, Art. no. 12334.

[38] X. Lin, Y. Xu, B. Zhang, R. Hao, H. Chen, and E. Li, "Unidirectional surface plasmons in nonreciprocal graphene," *New J. Phys.*, vol. 15, p. 113003, Nov. 2013.

[39] P. Li and T. Taubner, "Broadband subwavelength imaging using a tunable graphene-lens," *ACS Nano*, vol. 6, no. 11, pp. 10107–10114, 2012.

[40] B. H. Cheng, K. J. Chang, Y.-C. Lan, and D. P. Tsai, "Actively controlled super-resolution using graphene-based structure," *Opt. Exp.*, vol. 22, no. 23, pp. 28635–28644, 2014.

[41] P. B. Johnson and R. W. Christy, "Optical constants of the noble metals," *Phys. Rev. B, Condens. Matter*, vol. 6, no. 12, pp. 4370–4379, 1972.

[42] S. I. Jeon, J. H. Lee, J. D. Andrade, and P. G. De Gennes, "Protein—Surface interactions in the presence of polyethylene oxide: I. Simplified theory," *J. Colloid Interface Sci.*, vol. 142, no. 1, pp. 149–158, 1991.

[43] P. Tassin, T. Koschny, and C. M. Soukoulis, "Graphene for terahertz applications," *Science*, vol. 341, no. 6146, pp. 620–621, 2013.

[44] J. Hao, J. Wang, X. Liu, W. J. Padilla, L. Zhou, and M. Qiu, "High performance optical absorber based on a plasmonic metamaterial," *Appl. Phys. Lett.*, vol. 96, no. 25, p. 251104, 2010.

[45] W. Gao, J. Shu, C. Qiu, and Q. Xu, "Excitation of plasmonic waves in graphene by guided-mode resonances," *ACS Nano*, vol. 6, no. 9, pp. 7806–7813, Sep. 2012.